9594 *Biochemistry* **2010,** *49,* 9594–9603
DOI: 10.1021/bi101214t

BIOCHEMISTRY
including biophysical chemistry & molecular biology
Article

Stereoselective Disulfide Formation Stabilizes the Local Peptide Conformation in Nisin Mimics

Eleanor R. Turpin,[‡] Boyan B. Bonev,*[,§] and Jonathan D. Hirst*[,‡]

[‡]*School of Chemistry, University of Nottingham, Nottingham, U.K., and* [§]*School of Biomedical Sciences, University of Nottingham, Nottingham, U.K.*

Received July 31, 2010; Revised Manuscript Received September 29, 2010

ABSTRACT: Nisin is a polymacrocyclic peptide antimicrobial with high activity against Gram-positive bacteria. Lanthionine and methyllanthionine bridges, closing the macrocycles, are stabilized by thioether bonds, formed between cysteines and dehydrated serine or threonine. The role of polypeptide backbone conformation in the formation of macrocycles A and B within cysteine mutants of nisin residues 1−12 is investigated here by molecular dynamics simulations. Enantiomeric combinational space of Cys3 and Cys7 and of Cys8 and Cys11 is examined for the preference of disulfide bond formation over helical turn formation within this region. A clear preference for spontaneous disulfide formation and closure of rings 3,7 and 8,11 is demonstrated for the D-Cys3, D-Cys7, L-Cys8, L-Cys11 nisin homologue, while interlinked rings A and B are obtained through disulfide bridges between L-Cys3 and D-Cys8 and between D-Cys7 and D-Cys11. This study offers a simple designer approach to solid phase synthesis of macrocyclic peptides and lantibiotic analogues.

The management of infectious diseases remains a challenge in modern healthcare. Resistance to all classes of clinically relevant antibiotics has been reported, with more than 50% of *Streptococcus pneumoniae* and *Staphylococcus aureus* resistant to penicillin. Because very few new classes of antibiotics have been introduced recently, promising novel compounds are sought among antimicrobial peptides with specific targeted antibacterial action. Nisin is a peptide antibiotic with high efficiency against Gram-positive bacteria (*1*) and no human toxicity. It was discovered as early as 1928 (*2*) and has been in industrial use since the 1950s (*3*) . Its 34-amino acid residue structure contains five macrocyclic rings stabilized by thioether bonds, common in compounds belonging to the class of lanthionine antibiotics. Nisin binds to negatively charged lipid membranes (*4*), where it targets pyrophosphate-containing bacterial cell wall intermediates lipid II and undecaprenyl pyrophosphate (11PP) (*5*). Nisin forms lytic complexes with lipid II (*6*) and cell wall inhibitory complexes with 11PP (*5*), and it interferes with cell shape regulation and bacterial division (*7*). Target recognition is mediated by nisin residues 1−12 (*8*), while residues 13−34 are important in pore formation.

Nisin is ribosomally synthesized with a leader sequence comprising a 57-residue linear peptide containing serine and threonine residues, which are dehydrated after translation to dehydroalanine and dehydrobutyric acid by the dehydratase NisB. The lanthionine and methyllanthionine rings are formed by a cyclase, NisC, and the peptide is exported across the plasma membrane by an ABC transporter, NisT (*9*, *10*), at which point the leader peptide is removed to yield active nisin. It has been suggested that NisB, NisC, and NisT function as a membrane-associated complex (*11*). The biosynthesis of a related lanthionine antibiotic, subtilin from *Bacillus subtilis*, has been described involving a similar protein complex, SpaB, SpaC, and SpaT (*12*).

Commercial production of nisin relies exclusively on biosynthesis using *Lactococcus lactis* (*3*). Considering the industrial importance of the peptide, numerous strategies for obtaining chemisynthetic analogues have been developed over the years. These, however, remain industrially impractical. Challenges in the synthetic approach have been tackled, and techniques have been proposed for the synthesis of dehydrated residues (*13*), methyllanthionine (*14*, *15*) and lanthionine (*15*). Multistep synthesis of nisin from disulfide-cyclized analogues has also been described previously (*16*).

Ring C in nisin offers a good model for modifications, because of its relative isolation, and changes in this part of the molecule affecting antimicrobial activity can be attributed specifically to the conformation and integrity of that ring. Diastereomeric analogues of ring C, closed by lanthionine (*17*) and norlanthionine (*18*), have been synthesized, and their conformation has been studied. Alternative linkers for closing ring C have been considered, including alkene bridges (*19*) and alkyne bridges (*20*). Disulfide-linked ring C analogues of nisin have been prepared biosynthetically and exhibit antimicrobial activity (*21*).

The pyrophosphate recognition region of nisin includes two of the five macrocyclic rings (*8*), A:3−7 and B:8−11 (Figure 1). In this work, we investigate the conformation of peptide analogues of the first 12 residues of nisin, in which disulfide cysteines 3 and 7 and cysteines 8 and 11 are substituted for the thioether bonds in rings A and B (Figure 1b). The chirality of the cysteines 3, 7, 8, and 11 is altered to cover the enantiomer space, thus producing the set of 16 analogues listed in Table 1. Molecular dynamics (MD)[1] simulations of the set of analogues, without the disulfide

*To whom correspondence should be addressed. Phone: +44 115 9513478. Fax: +44 115 9513562. E-mail: jonathan.hirst@nottingham.ac.uk or boyan.bonev@nottingham.ac.uk.

[1]Abbreviations: MD, molecular dynamics; NMR, nuclear magnetic resonance; GBSW, generalized Born with simple switching; PMF, potential of mean force; rms, root-mean-square.

 Published on Web 09/30/2010

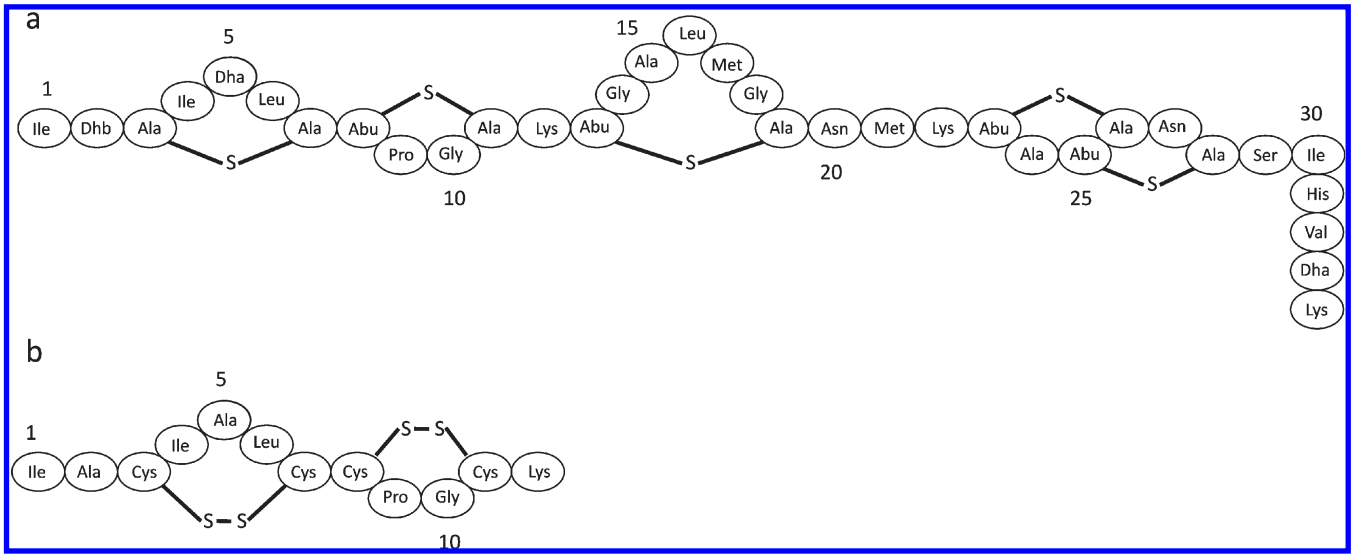

FIGURE 1: (a) Sequence of nisin showing the thioether rings and the unusual amino acids aminobutyric acid (Abu), dehydroalanine (Dha), and dehydrobutyrine (Dhb). (b) Sequence of the proposed disulfide analogue of the first 12 residues of nisin.

Table 1: Chirality of the Cysteine Residues in Each Nisin Analogue[a]

nisin analogue	Cys3	Cys7	Cys8	Cys11	nisin analogue	Cys3	Cys7	Cys8	Cys11
0	L	L	L	L	8	D	L	L	L
1	L	L	L	D	9	D	L	L	D
2	L	L	D	L	10	D	L	D	L
3	L	L	D	D	11	D	L	D	D
4	L	D	L	L	12	D	D	L	L
5	L	D	L	D	13	D	D	L	D
6	L	D	D	L	14	D	D	D	L
7	L	D	D	D	15	D	D	D	D

[a]The other residues are L-amino residues.

bonds between cysteine sulfur atoms, have been conducted to predict which analogues, if any, favor conformations in which disulfide bonds between Cys3 and Cys7 and between Cys8 and Cys11 can form. Intersulfur distances of < 5.5 Å have been used as an indication of high probability of spontaneous disulfide formation and ring closure.

There are three possible disulfide frameworks for peptides and proteins with four cysteine residues (CysI, CysII, CysIII, and CysIV) and two disulfide bonds: globular connectivity (CysI−CysIII and CysII−CysIV), ribbon connectivity (CysI−CysIV and CysII−CysIII), and bead connectivity (CysI−CysII and CysIII−CysIV) (*22*). Disulfide-rich peptides are produced by all classes of organisms, where they perform functions such as defense against insects for plants, defense against bacteria for animals, and regulatory functions (*23*). An important class of disulfide-rich peptides consists of conotoxins, toxins, and venom components produced by spiders, scorpions, and cone snails, which have been studied and characterized extensively as possible drug leads (*24*). The bead connectivity, which mimics the topology of the first two macrocyclic rings in nisin that are necessary for pyrophosphate recognition, has not been observed in nature (*23*) but has been made synthetically. Gehrmann et al. (*25*) synthesized all three isomers of a two-disulfide conotoxin and characterized them using NMR. The bead connectivity had a much less well-defined structure than the native globular and non-native ribbon connectivities, with a more stable N-terminus, a disordered C-terminus, and deviations from random coil values, indicating a highly solvent accessible backbone.

We are not aware of any studies in which thioether bonds have been substituted for disulfides, but there are examples of analogues in which disulfides have been replaced with thioethers. Bondebjerg et al. (*26*) synthesized thioether analogues of a conotoxin; the analogues were significantly less potent that the native conotoxin, but changes to the orientation of the thioether bonds are expected to increase potency. Levengood and van der Donk (*27*) used a cyclase that forms the thioether rings in the lantibiotic lacticin, by dehydration and cyclization, to synthesize a thioether analogue of a snake venom conotoxin but did not report its biological activity.

MD simulations on their own, and in combination with other computational techniques, have been used to study disulfide formation and bond shuffling. Schmid et al. (*28*) used MD simulations in explicit solvent to study disulfide bridge shuffling in bovine α-lactalbumin. To improve sampling, they used a representation of the cysteine residues with no constraints on bond length, bond angle, or dihedral angle. The simulations at 353 and 373 K favored a non-native disulfide bond that has been observed experimentally (*29*, *30*) as a folding intermediate and at elevated temperatures. Aschi et al. (*31*) performed MD simulations of two hepcidins, containing four disulfide bonds, in both reduced and oxidized states and found that the disulfide bonds are essential for maintaining the β-hairpin motif. Nilsson and co-workers (*32*−*35*) have used MD simulations in combination with pK_a calculations, quantum chemistry calculations, measured NMR scalar coupling constants, and experimentally determined pK_a values of selected residues to study the disulfide bond at the active site of the thioredoxin superfamily. The aim was to investigate how structure and protein environment result in a difference in redox potential across members of the family and the thiol−disulfide exchange reaction needed for dissociations of thioredoxin complexes.

The cysteine residue pattern, loop size, position of non-cysteine residues, backbone conformation, and preexisting disulfides all have important roles in forming native disulfide bonds (*23*), but how these factors interact varies between peptides. Information about the structure and dynamics of peptides and proteins can be obtained by NMR experiments, but analysis of disulfides by NMR can be difficult as intersulfur distances cannot be measured directly. Therefore, MD simulations are a useful tool for studying

how structure and dynamics contribute to the formation of disulfide bonds in the nisin analogues and in peptides more generally. The results of these simulations will be used to plan and conduct experimental work on the synthesis of nisin analogues.

METHODS

The peptide was built in CHARMM (*36*) with the amino acid sequence Ile-Ala-Cys-Ile-Ala-Leu-Cys-Cys-Pro-Gly-Cys-Lys. An acetyl N-terminus and methylamine C-terminus were added so that the termini were neutral. The lysine residue was positively charged. The initial conformation of the backbone was fully extended. The S_3-S_7 and S_8-S_{11} distances were 14.0 and 12.4 Å, respectively. We changed the chirality of the cysteine residues from L to D by deleting the side chain, exchanging the position of the C_β and H_α atoms, and rebuilding the side chain from the C_β atom. The molecules were energy minimized in vacuo using the steepest descent and adopted basis Newton−Raphson algorithms. MD simulations were performed using CHARMM version 34b1 with the CHARMM22 protein force field (*37*). The CMAP force field term (*38*), with an energetic correction to the peptide backbone, was not used because the correction is not defined for D-amino acids.

The generalized Born with simple switching (*39*) (GBSW) implicit solvent model was used to access a time scale longer than is available with explicit solvent models. The Born radii were those optimized by Nina et al. (*40*), and the GBSW model parameters were the recommended defaults. Yeh and Wallqvist (*41*) compared the effect of GBSW, another implicit solvent model, GBMV, and explicit solvent on peptide structure and dynamics; they concluded that structural properties sampled by the explicit solvent are reasonably represented by the implicit models, but dynamic properties were not as accurately represented, unless Langevin dynamics using a friction coefficient of 10 ps^{-1} was used. Feig (*42*) compared GBMV with explicit solvent in simulations of an alanine dipeptide, the B1 domain of streptococcal protein G, and ubiquitin using either a Nosé-Hoover thermostat or Langevin dynamics. Kinetics from Langevin dynamics with implicit solvent matched explicit solvent kinetics, but using a Nosé-Hoover thermostat with implicit solvent impeded the system's ability to cross energy barriers, because of the lack of stochastic collisions. Mor and Levy (*43*) studied proteins with long, flexible tails attached to their termini and reported that using a Berendsen thermostat caused a temperature difference between the tails and the rigid regions of secondary structure, but using a Langevin thermostat regulated the temperature of the inhomogeneous systems reliably. On the basis of these studies, Langevin dynamics with a friction coefficient of 10 ps^{-1} applied to nonhydrogen atoms was used to regulate temperature and include the effects of friction and collisions. For each nisin analogue, we conducted 10 independent runs of equilibration and production. The seed for the random number generator for the Langevin stochastic collisions was different for each independent run of each analogue, and the peptide was equilibrated at 298 K for 2 ns. The time step for equilibration and production was 1 fs, and the SHAKE algorithm (*44*) was used to constrain the lengths of bonds to hydrogen atoms. The production phase was 50 ns, and the positions of the atoms were recorded every 1 ps. Thus, a total of 0.5 μs of sampling was generated per analogue.

To understand how the chirality of the cysteine residues affects the formation of the disulfide bridges, we analyzed the backbone ϕ and ψ dihedral angles and hydrogen bonding patterns. Linear correlation coefficients were calculated between the sulfur−sulfur distance for each cysteine pair and the distance between the backbone amide hydrogen and backbone oxygen atoms for all possible residue combinations for each trajectory. A hydrogen−oxygen distance of < 2.4 Å indicates the formation of a hydrogen bond. Linear−circular correlation coefficients were calculated, using Mardia's method (*45*), between the sulfur−sulfur distance and each ϕ and ψ angle for each trajectory

$$r^2 = \frac{r_{yC}{}^2 + r_{yS}{}^2 - 2r_{yC}r_{yS}r_{CS}}{1 - r_{CS}{}^2} \quad (1)$$

where y represents the linear data, ϕ represents the circular data, r_{yC} is the correlation coefficient between y and cos ϕ, r_{yS} is the correlation coefficient between y and sin ϕ, and r_{CS} is the correlation coefficient between cos ϕ and sin ϕ. The range of r is 0−1, because positive and negative correlation cannot be distinguished in the circular−linear case. If a variable (H−O distance, ϕ, or ψ) and a sulfur−sulfur distance were correlated over five or more trajectories, with a coefficient of > 0.5, the correlation was investigated further.

RESULTS

To assess the thermodynamic stability of the simulations, the temperature and total energy as a function of time were examined and were stable during all the simulations (data not shown). All six sulfur−sulfur distances (S_3-S_7, S_3-S_8, S_3-S_{11}, S_7-S_8, S_7-S_{11}, and S_8-S_{11}) were recorded for each independent trajectory of each nisin analogue, and the associated distributions were calculated with an interval of 0.1 Å. Subject to the sufficiency of the conformational sampling, the histograms can be used to calculate the effective energy, or potential of mean force (PMF), of different conformational states as a function of sulfur−sulfur separation, using the Boltzmann relation in eq 2

$$N_i = N_0 \exp\left(-\frac{\Delta E_i}{k_B T}\right) \quad (2)$$

where N_0 is the number of conformations in the most populated, ground state, N_i is the number of conformations in the ith state, ΔE_i is the effective energy difference between the ground state and the ith state, k_B is the Boltzmann constant, and T is the temperature.

Figure 2 shows some typical histograms and the corresponding PMFs. The probability of the sulfur−sulfur distance being less than 5.5 Å, the cutoff for disulfide bridge formation, was calculated for the S_3-S_7 and S_8-S_{11} interactions, $P(S_3-S_7)$ and $P(S_8-S_{11})$.

Table 2 summarizes the effect of the chirality of Cys3 and Cys7 on the energetics of the S_3-S_7 interaction and $P(S_3-S_7)$, the probability of the S_3-S_7 distance being less than 5.5 Å. For seven of the analogues in which Cys3 is the L-enantiomer (nisin analogues 1−7), there is either no minimum or a shallow local minimum, corresponding to the possible formation of the S_3-S_7 disulfide bridge, and $P(S_3-S_7)$ is quite low, between 0.03 and 0.12. Analogue 0 has a deep local minimum when the S_3-S_7 distance is 5.0 Å and has a higher $P(S_3-S_7)$ of 0.18. Changing the chirality of Cys7 from the L-enantiomer (analogues 0−3) to the D-enantiomer (analogues 4−7) decreases $P(S_3-S_7)$.

Six of the analogues with D-Cys3 favor the formation of the S_3-S_7 disulfide bridge. Two analogues in which Cys3 is the D-enantiomer and Cys7 is the L-enantiomer (analogues 10 and 11) and two analogues in which both Cys3 and Cys7 are the D-enantiomer (analogues 14 and 15) have a global energy minimum

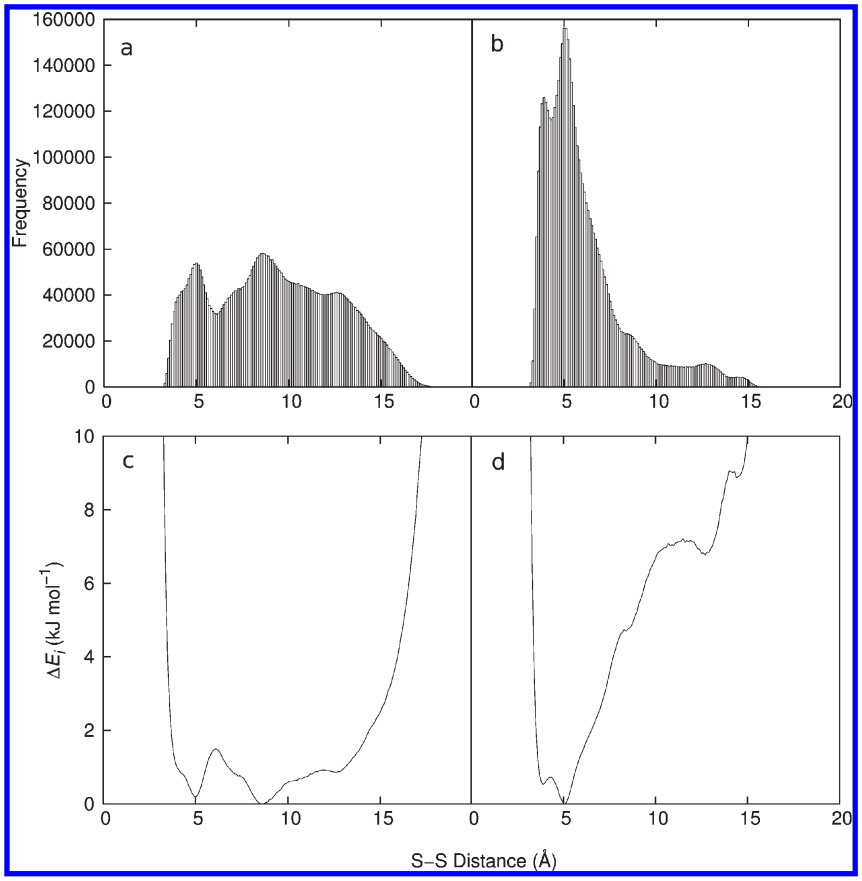

FIGURE 2: Histograms (top) and corresponding potentials of mean force (bottom) with respect to the S_3-S_7 (a and c) and S_8-S_{11} (b and d) separations for nisin analogue 0, with four L-Cys residues.

Table 2: Effect of Cys3 and Cys7 Chirality on the PMF Surface and Probability of S_3 and S_7 Being Sufficiently Close in Space To Form a Disulfide Bridge[a]

nisin analogue	cysteine chirality	ΔE at 5.5 Å (kJ/mol)	$P(S_3-S_7)$	location of the first minimum (Å)
0	L-Cys3−L-Cys7	0.9	0.18	5.0 (0.2 kJ/mol)
1		2.2	0.12	4.7 (1.6 kJ/mol)
2		1.1	0.08	7.8
3		2.5	0.11	8.4
4	L-Cys3−D-Cys7	2.7	0.10	7.6
5		4.2	0.04	5.2 (3.9 kJ/mol)
6		6.0	0.03	7.6
7		4.1	0.09	3.8 (2.8 kJ/mol)
8	D-Cys3−L-Cys7	2.6	0.08	5.1 (2.3 kJ/mol)
9		0.8	0.15	5.3 (0.7 kJ/mol)
10		0.7	0.31	5.1
11		0.3	0.31	5.1
12	D-Cys3−D-Cys7	1.2	0.29	3.9 (0.6 kJ/mol)
13		1.8	0.23	3.7 (0.3 kJ/mol)
14		0.5	0.28	4.9
15		2.4	0.36	4.0

[a] ΔE at 5.5 Å is the value of PMF when S_3 and S_7 are thought to be close enough in space to form a disulfide bridge; $P(S_3-S_7)$ is the probability of the sulfur−sulfur separation being less than 5.5 Å, and the location of the first minimum gives the sulfur−sulfur separation of the first minimum on the PMF surface, with its value in parentheses if it is not the global minimum.

corresponding to the possible formation of the S_3-S_7 disulfide bridge, and $P(S_3-S_7)$ is between 0.28 and 0.36. The other two analogues in which both Cys3 and Cys7 are the D-enantiomer (analogues 12 and 13) have deep local minima that correspond to the formation of the S_3-S_7 disulfide bridge, and $P(S_3-S_7)$ is between 0.23 and 0.29. Analogues 8 and 9 have a lower $P(S_3-S_7)$ than the other D-Cys3 analogues (0.08 and 0.15), and the global energy minima are 13.4 and 13.5 Å, respectively, compared with values between 4.0 and 8.9 Å for the other 14 analogues. Figure 3 shows two PMFs as a function of S_3-S_7 distance. Analogue 5 has an L-Cys3−D-Cys7 pair and does not have a minimum corresponding to the S_3-S_7 interaction. Analogue 11 has a D-Cys3−L-Cys7 pair and has a minimum corresponding to the sulfur−sulfur interaction.

The formation of the S_3-S_7 bridge in analogues 10−15 corresponds to a type IV β-turn between residues 3 and 6. A type IV β-turn is defined as four consecutive residues in which the distance between the C_α atoms of the first and fourth residues is less than 7 Å and the ϕ and ψ dihedral angles of the central residues do not fit the criteria of the standard turn types or helices (*46*). The correlation analysis did not identify any backbone hydrogen bonds or dihedral angles associated with the S_3-S_7 disulfide bridge. For analogues 10−15, the S_3-S_7 bridge can form in 29% of trajectory frames; 76% of these frames, or 22% of the total frames, correspond to a $C_{\alpha3}-C_{\alpha6}$ distance of <7 Å. For analogues 0−9, the fraction of frames in which both the S_3-S_7 distance is less than 5.5 Å and the $C_{\alpha3}-C_{\alpha6}$ distance is less than 7 Å is 5%. The mean average values of the central residues' (ϕ and ψ) angles are $-90 \pm 20°$ and $-65 \pm 31°$ for Ile4 and $-95 \pm 21°$ and $-77 \pm 32°$ for Ala5, respectively. These averages are calculated across analogues 10−15 when the S_3-S_7 distance is less than 5.5 Å. The $C_{\alpha3}-C_{\alpha6}$ distance and ϕ and ψ angles confirm that D-Cys3-Ile4-Ala5-Leu6 adopts a type IV β-turn when the S_3-S_7 disulfide bridge can form.

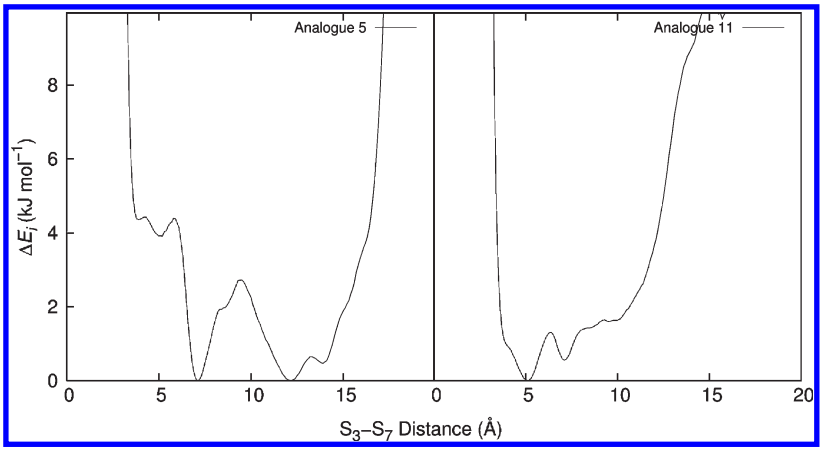

FIGURE 3: Examples of the potential of mean force as a function of the S_3-S_7 separation: (left) analogue 5 (L-Cys3−D-Cys7−L-Cys8−D-Cys11) and (right) analogue 11 (D-Cys3−L-Cys7−D-Cys8−D-Cys11).

Table 3: Effect of Cys8 and Cys11 Chirality on the PMF Surface and Probability of Cys8(S) and Cys11(S) Being Sufficiently Close in Space To Form a Disulfide Bridge[a]

nisin analogue	cysteine chirality	ΔE at 5.5 Å (kJ/mol)	$P(S_8-S_{11})$	location of the first minimum (Å)
0	L-Cys8−L-Cys11	0.6	0.54	5.0
4		0.4	0.49	5.2
8		0.5	0.25	5.1
12		0.4	0.32	5.2
1	L-Cys8−D-Cys11	1.3	0.19	5.1 (0.8 kJ/mol)
5		2.4	0.07	8.7
9		2.3	0.18	5.2 (2.0 kJ/mol)
13		1.0	0.18	5.1 (0.7 kJ/mol)
2	D-Cys8−L-Cys11	2.2	0.07	6.9
6		5.3	0.02	7.4
10		1.1	0.11	8.0
14		4.1	0.03	10.7
3	D-Cys8−D-Cys11	1.7	0.08	9.5
7		7.7	0.01	9.6
11		2.4	0.06	9.4
15		6.9	0.01	12.0

[a] ΔE at 5.5 Å is the value of the PMF when S_8 and S_{11} are thought to be close enough in space to form a disulfide bridge; $P(S_8-S_{11})$ is the probability of the sulfur−sulfur separation being less than 5.5 Å, and the location of first minimum gives the sulfur−sulfur separation of the first minimum on the PMF surface, with its value in parentheses if it is not the global minimum.

The effect of the chirality of Cys8 and Cys11 on the energetics of the S_8-S_{11} interaction and on $P(S_8-S_{11})$ is summarized in Table 3. The nisin analogues with Cys8 and Cys11 as L-amino acids (0, 4, 8, and 12) favor the formation of the S_8-S_{11} disulfide bridge with the global energy minimum corresponding to the possible formation of the bridge and a $P(S_8-S_{11})$ value between 0.32 and 0.54. When Cys11 is changed to a D-amino acid and Cys8 remains an L-amino acid (analogues 1, 5, 9, and 13), $P(S_8-S_{11})$ drops to between 0.07 and 0.19, and for three of the analogues, there are local energy minima corresponding to the S_8-S_{11} bridge, but not a global minimum; the bridge is able to form, but it is less likely than in the case of L-Cys8 and L-Cys11. A D-Cys8 stops the formation of the S_8-S_{11} disulfide bridge: analogues 2, 3, 6, 7, 10, 11, 14, and 15 have lower values for $P(S_8-S_{11})$ and no energy minima corresponding to the formation of the S_8-S_{11} bridge. Figure 4 contains examples of PMF as a function of S_8-S_{11} distance: analogue 4 (L-Cys8−L-Cys11), with a minimum corresponding to an S_8-S_{11} interaction, and analogue 7 (D-Cys8−D-Cys11) without.

A backbone hydrogen bond between the backbone carbonyl of Cys8 and the backbone amines of Cys11 and Lys12 was identified as being associated with the formation of the S_8-S_{11} disulfide bridge. Table 4 lists the average lifetimes, average occupancies, and numbers of trajectories at which the occupancy was greater than 1% for this hydrogen bond. For the analogues in which both Cys8 and Cys11 are L-amino acids, the formation of the Cys8−Cys11/Lys12 hydrogen bond brings Cys8 and Cys11 sufficiently close in space that the S_8-S_{11} distance is less than 5.5 Å and the disulfide bridge could form. In simulations of analogues 4 and 12, the hydrogen bond and the disulfide bridge contact form simultaneously for parts of nine of the independent trajectories; during the other trajectory, neither the hydrogen bond nor the disulfide bridge forms. Similarly, during simulations of analogue 8, the hydrogen bond is associated with the disulfide interaction for seven of the trajectories, and during the other three, neither forms. In simulations of analogue 0, the hydrogen bond and disulfide bridge contact are simultaneously formed for parts of all 10 independent trajectories.

A hydrogen bond with a lower occupancy forms between Cys8 and Cys11/Lys12 during simulations of L-Cys8−D-Cys11 analogues 1, 5, 9, and 13; occurrences of this hydrogen bond do correlate with instances of the S_8-S_{11} disulfide bridge contact. Although the average lifetime is similar to the simulations of the analogues in which both cysteines are L-amino acids, the lower occupancy reduces $P(S_8-S_{11})$ of the L-Cys8−D-Cys11 analogues, because there is no stabilizing hydrogen bond keeping S_8 and S_{11} close together.

Analogues with a D-Cys8 are unable to form the disulfide bridge contact between S_8 and S_{11}. During the simulations of the analogues with D-Cys8 and L-Cys11, the Cys8−Cys11/Lys12 hydrogen bond was able to form, but it brought S_7 and S_{11}, rather than S_8 and S_{11}, sufficiently close in space to form a disulfide bridge. For five of the trajectories of analogue 2 and four of the trajectories of analogue 14, Cys8 forms a stable hydrogen bond with Cys11 and Lys12, which is associated with the S_7-S_{11} disulfide bridge contact. For three of the trajectories of analogue 6, the Cys8−Cys11/Lys12 hydrogen bond brings S_7 and S_{11} together; for another three trajectories, the hydrogen bond forms between the carbonyl of Cys7 and the amine of Cys11. The interaction between S_7 and S_{11} may be blocked by the side chain of Cys8 when it is the L-enantiomer.

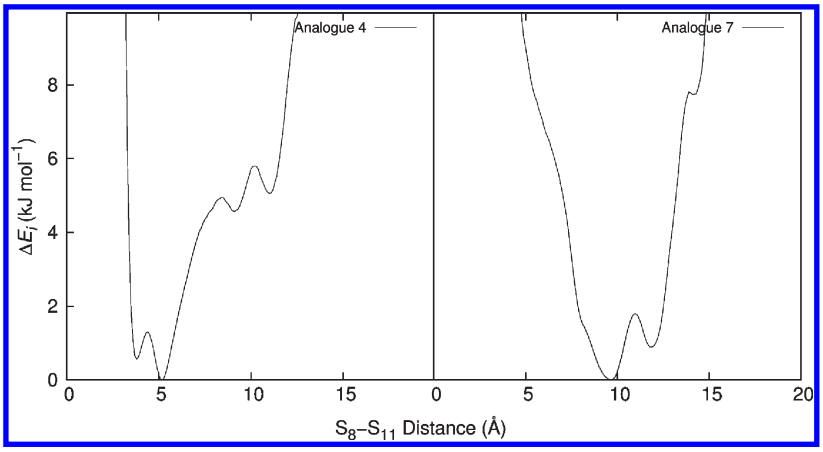

FIGURE 4: Examples of the potential of mean force as a function of the S_8−S_{11} separation: (left) analogue 4 (L-Cys3−D-Cys7−L-Cys8−L-Cys11) and (right) analogue 7 (L-Cys3−D-Cys7−D-Cys8−D-Cys11).

Table 4: Properties of the Cys8−Cys11(HN)/Lys12 Hydrogen Bond[a]

cysteine chirality	analogue	⟨lifetime⟩ (ps)	⟨occupancy⟩ (%)	no. of trajectories with an occupancy of >1%
L-Cys8−L-Cys11	0	14	56	10
	4	15	61	9
	8	11	17	9
	12	13	53	7
L-Cys8−D-Cys11	1	13	19	10
	5	11	26	10
	9	9	11	10
	13	10	15	9
D-Cys8−L-Cys11	2	9	31	5
	6	9	14	5
	10	21	80	10
	14	11	25	4
D-Cys8−D-Cys11	3	4	3	6
	7	4	1	4
	11	7	5	8
	15	6	2	4

[a]The ⟨lifetime⟩ is the mean lifetime of the hydrogen bond; the ⟨occupancy⟩ is the mean percentage of frames during which the hydrogen bond forms.

Analogue 10 has a high occupancy (80%) and mean lifetime (21 ps) of the hydrogen bond compared with the other analogues. Although the Cys8−Cys11/Lys12 hydrogen bond does correspond to the S_7−S_{11} interaction in analogue 10, the hydrogen bond is much more stable than the sulfur−sulfur interaction. Analogue 10 has a high probability of formation of the S_3−S_{11} disulfide bridge [$P(S_3$−$S_{11})$ = 0.59] compared with the other 15 analogues, where $P(S_3$−$S_{11})$ is between 0.04 and 0.38 and the mean value is 0.16. The Cys8−Cys11/Lys12 hydrogen bond corresponds to the S_3−S_{11} disulfide bridge for parts of nine of the 10 trajectories of analogue 10. The Cys8−Cys11/Lys12 hydrogen bond brings Cys11 close to Cys7, and the D-Cys3-Ile4-Ala5-Leu6 type IV β-turn brings Cys3 close to Cys7 and therefore close to Cys11. During the simulations of the analogues with D-Cys8 and D-Cys11, the Cys8−Cys11/Lys12 hydrogen bond has low mean lifetimes (4−7 ps) and low occupancies (1−5%) compared with the other analogues and $P(S_8$−$S_{11})$ is low.

During the simulations of the analogues with L-Cys8 and L-Cys11, residues 8−11 form a type IV β-turn. Across analogues 0, 4, 8, and 12, the average percentage of trajectory frames in which the S_8−S_{11} bridge can form is 40%; 97% of these frames correspond to a $C_{\alpha 8}$−$C_{\alpha 11}$ distance of < 7 Å. The average values of the central residues' ϕ and ψ angles, which characterize a β-turn, are −72 ± 9° and −29 ± 70° for Pro9 and −128 ± 78° and −34 ± 42° for Gly10, respectively. These averages are calculated across all analogues with L-Cys8 and L-Cys11 when the S_8−S_{11} distance is less than 5.5 Å and the uncertainty is the angular deviation.

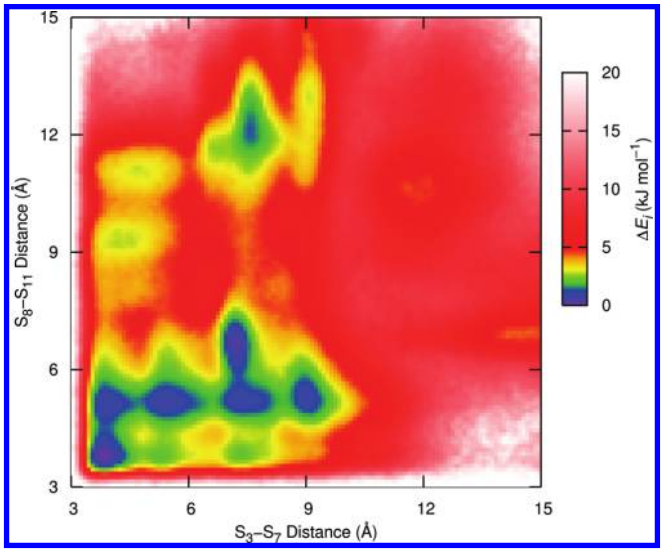

FIGURE 5: Potential of mean force as a function of S_3−S_7 and S_8−S_{11} separation (bead connectivity) for nisin analogue 12.

Three-dimensional histograms of S_3−S_7 and S_8−S_{11} distances with an interval of 0.1 Å were used to produce PMF surfaces using the Boltzmann relation. Figure 5 is the PMF for S_3−S_7 and S_8−S_{11} distances for analogue 12 has a global minimum at (3.8 Å, 3.8 Å), corresponding to the bead connectivity. The S_3−S_7 and S_8−S_{11} distances during the nisin analogue 12 trajectories were checked every 2.0 ps and the atomic coordinates written for those that corresponded to the bead connectivity. The resulting conformations were clustered using the kclust module in MMTSB (*47*), and Figure 6 shows the centroid of the most populated cluster. Analogues 7 and 13 are not able to form the bead connectivity but do have a global minimum corresponding to the globular connectivity at (5.0 Å, 5.0 Å) and at (3.7 Å, 4.6 Å), respectively (Figures 7 and 8). Figure 9 shows the centroid of the most populated cluster from clustering of trajectory frames,

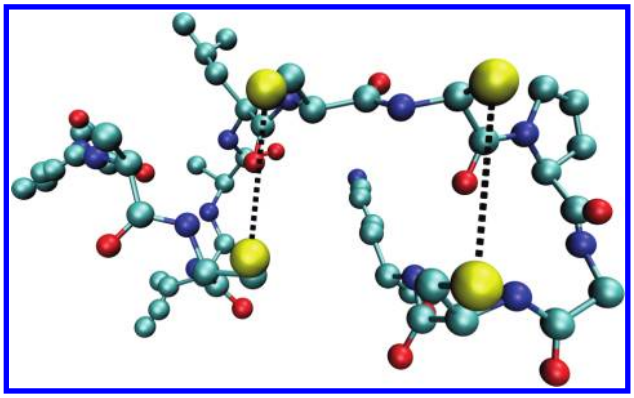

FIGURE 6: Centroid of the most populated cluster from clustering of trajectory frames from the simulations of nisin analogue 12, which corresponded to bead connectivity.

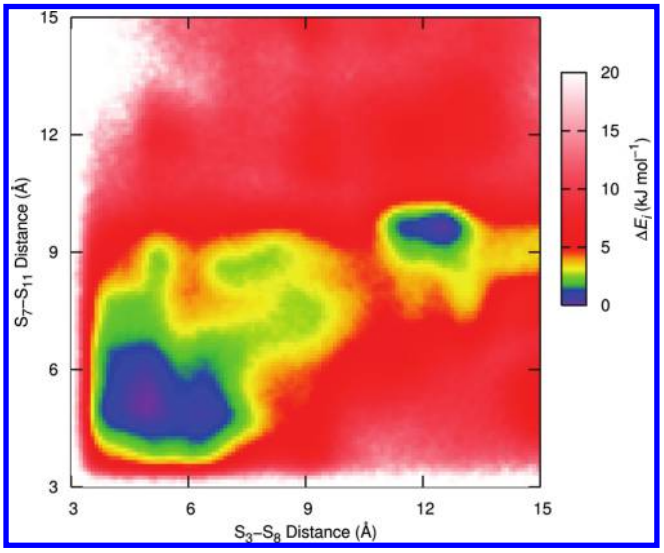

FIGURE 7: Potential of mean force as a function of S_3-S_8 and S_7-S_{11} separation (globular connectivity) for nisin analogue 7.

corresponding to the globular connectivity, from the simulations of nisin analogue 13.

The rms differences between the peptide backbone atoms of the first 12 residues of the NMR structure of nisin in complex with lipid II (*8*) (Protein Data Bank entry 1WCO) and the centroids of the four most populated clusters calculated for nisin analogue 12 are listed in Table 5. When the rms difference from 1WCO is calculated with respect to all the residues, residues 1−12, or excluding the termini, residues 2−11, the deviation is quite high. However, just using the thioether/disulfide rings and neglecting the flexible linking residues, we found the rms difference for residues 3−7 is less than 1.7 Å for clusters 2−4 and 1.1 Å for cluster 1. For residues 8−11, it is 1.0 Å for cluster 1 and less than 0.7 Å for clusters 2−4. Figure 10 shows an alignment of backbone atoms for residues 3−7 between 1WCO and cluster 1, and Figure 11 shows an alignment of backbone atoms for residues 8−11 between 1WCO and clusters 2−4. The hydrogen bonding of the centroids of the four most populated clusters was also examined. Clusters 2−4 have hydrogen bonds between the carbonyl of Cys8 and the backbone amines of Cys11 and Lys12 and between the carbonyl of Cys3 and the amines of Leu6 and Cys7. Cluster 1 has hydrogen bonds between the carbonyl of Cys8 and the amines of Cys11 and Lys12, the carbonyl of Ile1 and the amines of Ala5 and Leu6, the carbonyl of Leu6 and the amine

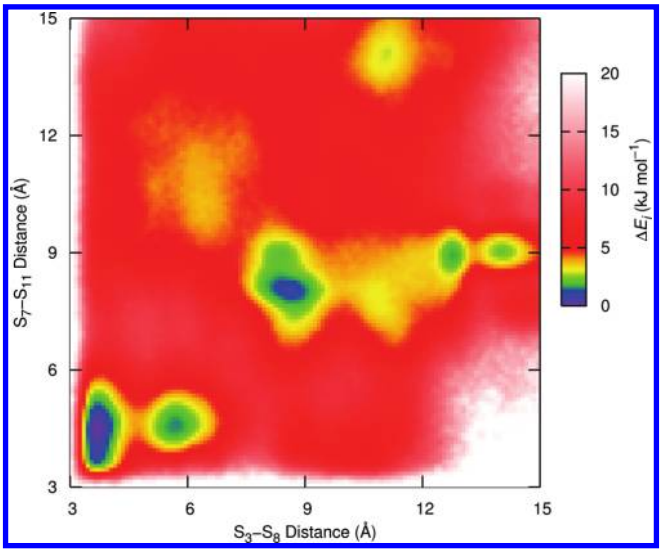

FIGURE 8: Potential of mean force as a function of S_3-S_8 and S_7-S_{11} separation (globular connectivity) for nisin analogue 13.

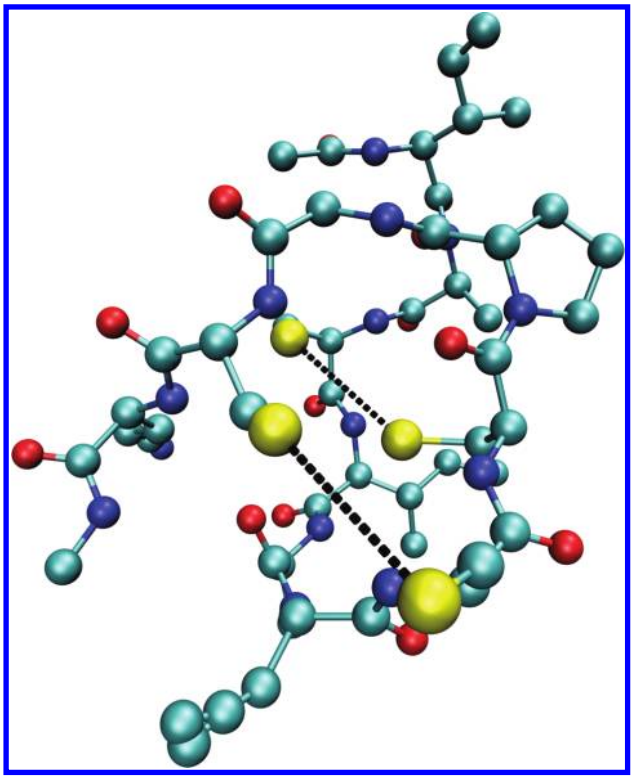

FIGURE 9: Centroid of the most populated cluster from clustering of trajectory frames from the simulations of nisin analogue 13, which corresponded to globular connectivity.

of Cys3, and the carbonyl of Ala5 and the side chain of Lys12. Clusters 2−4 are very similar and differ only in the position of the N-terminus. Cluster 1 is different from the other top three clusters, with the extra hydrogen bonds among the N-terminus, the C-terminus, and Ala5 leading to "tucked in" termini.

DISCUSSION

Mitchell and Smith (*48*) surveyed all peptide and protein entries in the Protein Data Bank for D-amino acid residues and observed that D-amino acid residues in L-amino acid chains have a propensity for forming β-turns. Of a representative subset of 40 D-amino acid residues in L-amino chains, where duplicate

Table 5: rms Differences between the Peptide Backbone Atoms of the Centroids of the Four Most Populated Clusters of Nisin Analogue 12 and 1WCO[a]

	rms difference from 1WCO (Å)			
cluster (percentage of structures)	residues 3−7	residues 8−11	residues 2−11	residues 1−12
1 (30.0%)	1.1	1.0	3.5	4.5
2 (18.2%)	1.6	0.6	2.6	3.1
3 (13.5%)	1.7	0.6	2.6	3.0
4 (9.4%)	1.6	0.7	2.8	3.7

[a]The percentage of conformations assigned to each cluster is shown in parentheses.

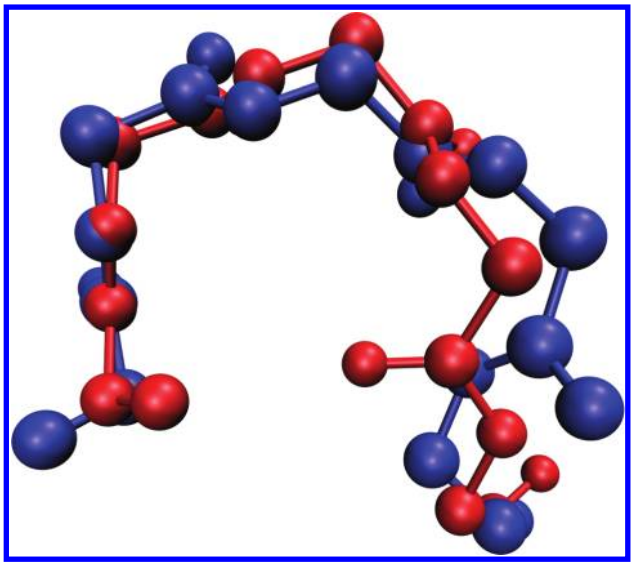

FIGURE 10: Alignment of backbone atoms for residues 3−7 between 1WCO (blue) and the centroid of cluster 1 (red) for nisin analogue 12.

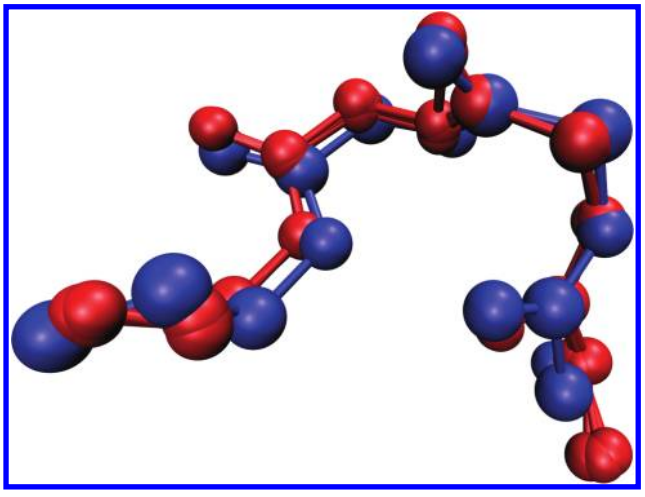

FIGURE 11: Alignment of backbone atoms for residues 8−11 between 1WCO (blue) and the centroids of clusters 2−4 (red) of nisin analogue 12.

sequences had been removed, 17 of the residues were involved in a β-turn, the majority of which were classed as nonstandard, or type IV. The formation of the 3−6 β-turn when Cys3 is a D-amino acid residue brings the sulfur atoms in Cys3 and Cys7 sufficiently close in space to form a disulfide bridge, for two of the L-Cys7 analogues (10 and 11) and all of the D-Cys7 analogues (12−15). When the Cys3 is an L-amino acid, the 3−6 β-turn does not form and $P(S_3-S_7)$ is reduced.

Ring B is conserved across type A lantibiotics (*8*), and a hydrogen bond similar to the Cys8−Cys11/Lys12 hydrogen bond has been observed during NMR experiments: between D-Ala8 and Gly10 and Ala11 in nisin (*49*), between D-Ala8 and Ala11 in gallidermin (*50*), and between D-Ala8 and Gly10 and Ala11 in mutacin 1140 (*51*). Ring B is described as a type II β-turn for the nisin and gallidermin structures (*49*, *50*) and alternates between a type II and type I β-turn for the mutacin 1140 structure (*51*). Hsu et al. (*52*) substituted different amino acids into a β-hairpin scaffold between cysteine residues to study their propensity for forming β-turns and found that Cys-Pro-Gly-Cys particularly favors β-turn formation. Proline and glycine are residues 9 and 10, respectively, in the nisin analogues.

In the simulations of the nisin analogues, the S_8-S_{11} disulfide interaction is more stable than the S_3-S_7 disulfide interaction. The S_8-S_{11} interaction is stabilized by the hydrogen bond between Cys8 and Cys11/Lys12 and by the amino acid sequence Cys-Pro-Gly-Cys, which favors a β-turn conformation. Another factor in the difference between the S_8-S_{11} and S_3-S_7 interactions is that the stability of small disulfide loops depends on whether the number of residues between the cysteines is odd or even. Zhang and Snyder (*53*) measured the microscopic disulfide exchange rate constants for C-X_m-C peptides, where m is the number of residues between the cysteines. They found that an even value of m favors disulfide bond formation more than an odd value, with m values of 2 and 4 most favored for m values of ≤ 5.

CONCLUSION

Peptide analogues of nisin target recognition region of residues 1−12, rings A and B, were constructed in silico, and their conformation was examined using MD simulations. Virtual screening of peptide conformations was performed using the estimated ability of cysteine analogues to engage in pairwise disulfide bond formation between side chains of different enantiomeric cysteine residues. Good convergence in the simulations in all peptides indicates a clearly preferred backbone conformation of the peptide. This suggests that the chain in nascent prenisin has a favorable conformation, which readily presents activated groups for cyclization by the cyclase NisC. We also conclude that strategic stereoselective cysteine mutations in nisin analogues can produce engineered macrocyclic peptides through spontaneous formation of disulfide bonds in solid phase-synthesized peptides.

ACKNOWLEDGMENT

We are grateful for access to the University of Nottingham High Performance Computing facility.

REFERENCES

1. Bonev, B., Hooper, J., and Parisot, J. (2008) Principles of assessing bacterial susceptibility to antibiotics using the agar diffusion method. *J. Antimicrob. Chemother. 61*, 1295–1301.
2. Rogers, L. A., and Whittier, E. O. (1928) Limiting factors in the lactic fermentation. *J. Bacteriol. 16*, 211–229.
3. Thomas, L. V., Clarkson, M. R., and Delves-Broughton, J. (2000) Nisin: In Natural Food Antimicrobial Systems, CRC Press, Boca Raton, FL.
4. Bonev, B. B., Chan, W. C., Bycroft, B. W., Roberts, G. C. K., and Watts, A. (2000) Interaction of the lantibiotic nisin with mixed lipid bilayers: A P-31 and H-2 NMR study. *Biochemistry 39*, 11425–11433.

5. Bonev, B. B., Breukink, E., Swiezewska, E., De Kruijff, B., and Watts, A. (2004) Targeting extracellular pyrophosphates underpins the high selectivity of nisin. *FASEB J. 18*, 1862–1869.
6. Breukink, E., Wiedemann, I., van Kraaij, C., Kuipers, O. P., Sahl, H. G., and de Kruijff, B. (1999) Use of the cell wall precursor lipid II by a pore-forming peptide antibiotic. *Science 286*, 2361–2364.
7. Hyde, A. J., Parisot, J., McNichol, A., and Bonev, B. B. (2006) Nisin-induced changes in *Bacillus* morphology suggest a paradigm of antibiotic action. *Proc. Natl. Acad. Sci. U.S.A. 103*, 19896–19901.
8. Hsu, S. T. D., Breukink, E., Tischenko, E., Lutters, M. A. G., de Kruijff, B., Kaptein, R., Bonvin, A., and van Nuland, N. A. J. (2004) The nisin-lipid II complex reveals a pyrophosphate cage that provides a blueprint for novel antibiotics. *Nat. Struct. Mol. Biol. 11*, 963–967.
9. van Saparoea, H. B. V., Bakkes, P. J., Moll, G. N., and Driessen, A. J. M. (2008) Distinct contributions of the nisin biosynthesis enzymes NisB and NisC and transporter NisT to prenisin production by *Lactococcus lactis*. *Appl. Environ. Microbiol. 74*, 5541–5548.
10. Lubelski, J., Khusainov, R., and Kuipers, O. P. (2009) Directionality and coordination of dehydration and ring formation during biosynthesis of the lantibiotic nisin. *J. Biol. Chem. 284*, 25962–25972.
11. Kuipers, A., Meijer-Wierenga, J., Rink, R., Kluskens, L. D., and Moll, G. N. (2008) Mechanistic dissection of the enzyme complexes involved in biosynthesis of lacticin 3147 and nisin. *Appl. Environ. Microbiol. 74*, 6591–6597.
12. Helfrich, M., Entian, K. D., and Stein, T. (2007) Structure-function relationships of the lanthionine cyclase SpaC involved in biosynthesis of the *Bacillus subtilis* peptide antibiotic subtilin. *Biochemistry 46*, 3224–3233.
13. Dey, S., Vijayaraghavan, R., Goel, V. K., Kumar, S., Kumar, P., and Singh, T. P. (2005) Design rules for peptides with α,β-dehydro-residues: Synthesis of a model peptide Boc-Ile-ΔAla-OCH_3 and its crystal structures obtained from two different solvents. *J. Mol. Struct. 737*, 109–116.
14. Zhou, H., and van der Donk, W. A. (2002) Biomimetic stereoselective formation of methyllanthionine. *Org. Lett. 4*, 1335–1338.
15. Cobb, S. L., and Vederas, J. C. (2007) A concise stereoselective synthesis of orthogonally protected lanthionine and β-methyllanthionine. *Org. Biomol. Chem. 5*, 1031–1038.
16. Fukase, K., Kitazawa, M., Sano, A., Shimbo, K., Horimoto, S., Fujita, H., Kubo, A., Wakamiya, T., and Shiba, T. (1992) Synthetic study on peptide antibiotic nisin. 5. Total synthesis of nisin. *Bull. Chem. Soc. Jpn. 65*, 2227–2240.
17. Bregant, S., and Tabor, A. B. (2005) Orthogonally protected lanthionines: Synthesis and use for the solid-phase synthesis of an analogue of nisin ring C. *J. Org. Chem. 70*, 2430–2438.
18. Mustapa, M. F. M., Harris, R., Esposito, D., Chubb, N. A. L., Mould, J., Schultz, D., Driscoll, P. C., and Tabor, A. B. (2003) Synthesis of a cyclic peptide containing norlanthionine: Effect of the thioether bridge on peptide conformation. *J. Org. Chem. 68*, 8193–8198.
19. Ghalit, N., Kemmink, J., Hilbers, H. W., Versluis, C., Rijkers, D. T. S., and Liskamp, R. M. J. (2007) Step-wise and pre-organization induced synthesis of a crossed alkene-bridged nisin Z DE-ring mimic by ring-closing metathesis. *Org. Biomol. Chem. 5*, 924–934.
20. Ghalit, N., Poot, A. J., Furstner, A., Rijkers, D. T. S., and Liskamp, R. M. J. (2005) Ring-closing alkyne metathesis approach toward the synthesis of alkyne mimics of thioether A-, B-, C-, and DE-ring systems of the antibiotic nisin Z. *Org. Lett. 7*, 2961–2964.
21. van Kraaij, C., Breukink, E., Rollema, H. S., Bongers, R. S., Kosters, H. A., de Kruijff, B., and Kuipers, O. P. (2000) Engineering a disulfide bond and free thiols in the lantibiotic nisin Z. *Eur. J. Biochem. 267*, 901–909.
22. Daly, N. L., and Craik, D. J. (2009) Folding motifs of cysteine-rich peptides. In Oxidative folding of peptides and proteins (Buchner, J., and Moroder, L., Eds.) The Royal Society of Chemistry, Cambridge, U.K.
23. Bulaj, G., and Walewska, A. (2009) Oxidative folding of single-stranded disulfide-rich peptides. In Oxidative folding of peptides and proteins (Buchner, J., and Moroder, L., Eds.) The Royal Society of Chemistry, Cambridge, U.K.
24. Livett, B. G., Gayler, K. R., and Khalil, Z. (2004) Drugs from the sea: Conopeptides as potential therapeutics. *Curr. Med. Chem. 11*, 1715–1723.
25. Gehrmann, J., Alewood, P. F., and Craik, D. J. (1998) Structure determination of the three disulfide bond isomers of α-conotoxin GI: A model for the role of disulfide bonds in structural stability. *J. Mol. Biol. 278*, 401–415.
26. Bondebjerg, J., Grunnet, M., Jespersen, T., and Meldal, M. (2003) Solid-phase synthesis and biological activity of a thioether analogue of conotoxin G1. *ChemBioChem 4*, 186–194.
27. Levengood, M. R., and van der Donk, W. (2008) Use of lantibiotic synthetases for the preparation of bioactive constrained peptides. *Bioorg. Med. Chem. 18*, 3025–3028.
28. Schmid, N., Bolliger, C., Smith, L. J., and van Gunsteren, W. F. (2008) Disulfide bond shuffling in bovine α-lactalbumin: MD simulation confirms experiment. *Biochemistry 47*, 12104–12107.
29. Chang, J.-Y., and Li, L. (2001) The structure of denatured α-lactalbumin elucidated by the technique of disulfide scrambling: Fraction of conformational isomers of α-lactalbumin. *J. Biol. Chem. 276*, 9705–9712.
30. Chang, J.-Y. (2002) The folding pathway of α-lactalbumin elucidated by the technique of disulfide scrambling: Isolation of on-pathway and off-pathway intermediates. *J. Biol. Chem. 277*, 120–126.
31. Aschi, M., Bozzi, A., Di Bartolomeo, R., and Petruzzelli, R. (2010) The role of disulfide bonds and N-terminus in the structural properties of hepcidins: Insights from molecular dynamics simulations. *Biopolymers 93*, 917–926.
32. Foloppe, N., Sagemark, J., Nordstrand, K., Berndt, K. D., and Nilsson, L. (2001) Structure, dynamics and electrostatics of the active site of glutaredoxin 3 from *Escherichia coli*: Comparison with functionally related proteins. *J. Mol. Biol. 310*, 449–470.
33. Foloppe, N., and Nilsson, L. (2004) The glutaredoxin -C-P-Y-C- motif: Influence of peripheral residues. *Structure 12*, 289–300.
34. Foloppe, N., and Nilsson, L. (2007) Stabilization of the catalytic thiolate in a mammalian glutaredoxin: Structure, dynamics and electrostatics of reduced pig glutaredoxin and its mutants. *J. Mol. Biol. 372*, 798–816.
35. Roos, G., Foloppe, N., van Laer, K., Wyns, L., Nilsson, L., Geerlings, P., and Messens, J. (2009) How thioredoxin dissociates its mixed disulfide. *PLoS Comput. Biol. 5*, e1000461.
36. Brooks, B. R., Bruccoleri, R. E., Olafson, D. J., States, D. J., Swaminathan, S., and Karplus, M. (1983) CHARMM: A program for macromolecular energy, minimization, and dynamics calculations. *J. Comput. Chem. 4*, 187–217.
37. MacKerell, A. D., Jr., Bashford, D., Bellott, M., Dunbrack, R. L., Evanseck, J. D., Field, M. J., Fischer, S., Gao, J., Guo, H., Ha, S., Joseph-McCarthy, D., Kuchnir, L., Kuczera, K., Lau, F. T. K., Mattos, C., Michnick, S., Ngo, T., Nguyen, D. T., Prodhom, B., Reiher, W. E., Roux, B., Schlenkrich, M., Smith, J. C., Stote, R. Straub, J., Watanabe, M., Wiorkiewicz-Kuczera, J., Yin, D., and Karplus, M. (1998) All-atom empirical potential for molecular modeling and dynamics studies of proteins. *J. Phys. Chem. B 102*, 3586–3616.
38. Mackerell, A. D., Jr., Feig, M., and Brooks, C. L., III (2004) Extending the treatment of backbone energetics in protein force fields: Limitations of gas-phase quantum mechanics in reproducing protein conformational distributions in molecular dynamics simulations. *J. Comput. Chem. 25*, 1400–1415.
39. Im, W. P., Lee, M. S., and Brooks, C. L. (2003) Generalized Born model with a simple smoothing function. *J. Comput. Chem. 24*, 1691–1702.
40. Nina, M., Beglov, D., and Roux, B. (1997) Atomic radii for continuum electrostatics calculations based on molecular dynamics free energy simulations. *J. Phys. Chem. B 101*, 5239–5248.
41. Yeh, I., and Wallqvist, A. (2009) Structure and dynamics of end-to-end loop formation of the penta-peptide Cys-Ala-Gly-Gln-Trp in implicit solvents. *J. Phys. Chem. B 113*, 12382–12390.
42. Feig, M. (2007) Kinetics from implicit solvent simulations of biomolecules as a function of viscosity. *J. Chem. Theory Comput. 3*, 1734–1748.
43. Mor, A., and Levy, G. Z. Y. (2008) Simulations of proteins with inhomogeneous degrees of freedom: The effect of thermostats. *J. Comput. Chem. 29*, 1992–1998.
44. Ryckaert, J. P., Ciccotti, G., and Berendsen, H. J. C. (1977) Numerical integration of the Cartesian equations of motion of a system with constraints: Molecular dynamics of n-alkanes. *J. Comput. Phys. 23*, 327–341.
45. Mardia, K. V. (1976) Linear-Circular Correlation Coefficients and Rhythmometry. *Biometrika 63*, 403–405.
46. Hutchinson, E. G., and Thornton, J. M. (1995) PROMOTIF: A program to identify and analyze structural motifs in proteins. *Protein Sci. 5*, 212–200.
47. Feig, M., Karanicolas, J., and Brooks, C. L., III (2001) MMTSB Tool Set, MMTSB NIH Research Resource, The Scripps Research Institute, La Jolla, CA.
48. Mitchell, J. B. O., and Smith, J. (2003) D-Amino acid residues in peptides and proteins. *Proteins: Struct., Funct., Bioinf. 50*, 563–571.
49. Van Den Hooven, H. W., Doeland, C. C. M., Van De Kamp, M., Konings, R. N. H., Hilbers, C. W., and Van De Ven, F. J. M. (1996) Three-dimensional structure of the lantibiotic nisin in the presence of membrane-mimetic micelles of dodecylphosphocholine and of sodium dodecylsulphate. *Eur. J. Biochem. 235*, 382–393.

50. Freund, S., Jung, G., Gutbrod, O., Folkers, G., Gibbons, W. A., Allgaier, H., and Werner, R. (1991) The solution structure of the lantibiotic gallidermin. *Biopolymers 31*, 803–811.
51. Smith, L., Zachariah, C., Thirumoorthy, R., Rocca, J., Novák, J., Hillman, J. D., and Edison, A. S. (2003) Structure and dynamics of the lantibiotic mutacin 1140. *Biochemistry 42*, 10372–10384.
52. Hsu, H.-J., Chang, H.-J., Peng, H.-P., Huang, S.-S., Lin, M.-Y., and Yang, A.-S. (2006) Assessing computational amino acid β-turn propensities with a phage-displayed combinatorial libray and directed evolution. *Structure 14*, 1499–1510.
53. Zhang, R., and Snyder, G. H. (1989) Dependence of formation of small disulfide loops in two-cysteine peptides on the number and types of intervening amino acids. *J. Biol. Chem. 264*, 18472–18479.